Journal of Univ of Sci and Tech Beijing
1997, Vol 4, No 2: 1

Comments on Quasicrystals*

MIN Lequan

Applied Science School, USTB, Beijing 100083, China

(Received in 1997-05-27)

Abstract: The discoveries of so-called quasicrystals have broken through the theoretic foundation set up by the classical crystallographic group theory since 1891 and proposed new topics for study of solid structures. Electron diffraction patterns (EDP's) and high-resolution microscopic (HREM) images have proved invaluable tools of studying the structures of crystals. The recognition and determination of EDP's and HREM images of a real-structure play a key role for understanding the structure. This paper will introduce some new developments about crystallographic group theory and new image processing methods on EDP's and HREM images. Contrary to popular beliefs, the research shows that quasicrystals can be understood (perturbed) complex periodic structures.

Key words: quasicrystals, nonclassical crystallographic groups, electron diffraction pattern, high-resolution microscopic image, high accuracy recognition, atomic models

A widely accepted assumption of the solid state is that the atomic structures of pure solids are either crystal structures or glassy structures. A crystal structure is a periodic structure, which consists of repeating atomic cluster called unit cell. However, a glassy structure is an aperiodic structure, which might consist of randomly packed atomic cluster. Modern theory of solid is founded on the science of classical crystallography, which is concerned with the enumeration of actual structures of various crystalline substances[1]. There are over 20 000 practical crystalline substances in the classical crystal kingdom. According to the classical crystallographic theory, a crystal structure can have n-fold rotational symmetry only if n = 2, 3, 4, or 6. As a result, the diffraction pattern of a crystal structure has only the same kind of rotational symmetries.

One important experimental evidence for the periodic arrangement of atoms in a crystal is corresponding diffraction patterns (produced with X-rays, electrons or neutrons) of crystals, which consist of groups of discrete bright spots whose diameters and positions represent the information of the corresponding crystal. Another important experimental evidence for the periodic arrangement of atoms in a crystal is corresponding high resolution electron microscopic images, in which bright specks whose distribution displays periodic characteristic might represent atom (atoms) columns of the corresponding crystal.

In 1984, Shechtman, Blech, Gratiaus and Cahn claimed to have discovered a new solid state matter in rapidly quenched Al-Mn alloy whose EDP has 5-fold rotational symmetry[2]. Following this discovery, many alloy phases with 5-, 8-, 10-, and 12-fold rotational symmetric EDP's consisting of discrete sharp peaks have been reported by different research groups for example see references [3 ~ 9]. Until now, several thousand papers in this field have been published. Now these metallic solids are called quasicrystals (QCs). Since the symmetries shown in the EDP's of QCs correspond to none of those in the 230 space groups described via the classical crystallography, these discoveries of QCs have challenged the widely held assumption of solid state and broken the theoretic foundation of the classical crystallography.

As early as in 1974, R. Penrose the Oxford particle physicist devised a mathematical game. In it a pair of quadrilateral shapes were used to tile a plane without translational periodicity, which is

*Financed by the Scientific Research Foundation and the Young Teacher Training Foundation of USTB

latterly named Penrose tiling[10]. In 1982, A. L. Mackey, a crystallographist at the University of London, reported that the optical diffraction effect of the Penrose tiling shows 5-fold rotational symmetry[11]. P. Steinhardt, D. Levine, and M. Duneau, A. Katz have, respectively, used generalized dual method[12,13] and high dimensional projection method[14] to generate (generalized) Penrose tilings whose Fourier Transform patterns (FTP's) show striking similarity with the EDP's of the 5-fold QC[2]. Shortly after Y. Watanabe et al. had presented the nonperiodic tessellation with 8-fold rotational symmetry[15], this tiling was used to explain the 8-fold QC[4].

The popular point of view is that QCs are a fundamentally new class of ordered nonperiodic structures. Many investigators have suggested that some aperiodic structures generated via the projections on 3-dimensional real space of periodic structures in higher dimensional spaces have discrete FTP's with strict 5-, 8-, 10-, and 12-fold symmetries which are similar to those displaying in the corresponding QCs (for example see references [4, 14, 16 ~ 19]). Practically some randomly packed models have also been used to interpret corresponding QCs (for example see references [20 ~ 22]). Mathematically, people think that three mathematical areas most relevant to quasicrysatals are the theory of almost periodic functions, the theory of aperiodic tilings, and the group theory[23]. Although a great many aperiodic QC models have been proposed, none of them has been generally accepted, in particular not one of them can explain all EDP's of the corresponding experimental QCs with 8-, 10- or 12-fold rotational symmetries. However a few have suggested that some twining models and/or crystal models can be used to explain some experimental observations (see references [24 ~ 32]).

HREM images of most quasicrystals do not seem to be periodic. But the corresponding EDP's appear to show good rotational 'symmetry'. If the idealized EDP's of the quasicrystals have 5-, 8-, 10-, and 12- fold rotational symmetry in the strict mathematical sense, then we can conclude that the HREM images imply that the corresponding quasicrystals are perturbed quasiperiodic structure. Therefore, the popular views on QCs are essentially right. However, the peaks in the diffraction patterns of some QCs with 12-fold rotational symmetry are not quite symmetrically arranged, small shifts occur[31,32]. Furthermore, on account of the imperfection of any method of measurement, it is impossible to claim whether an EDP of experimental alloy has n-fold symmetry in a strict mathematical sense. Consequently an EDP with approximate n-fold symmetry may be mistaken to exhibit n-fold symmetry in the strict mathematical sense. In fact we can also reasonably well assume that the diffraction dots in the idealized EDP's of the quasicrystals are located at corresponding integral lattice points in correspondings orthogonal coordinate systems or oblique coordinate systems. This means that the so-called QCs are essentially perturbed periodic structures but they do not belong to the classical crystallographic space groups because not one of the diffraction patterns of the space group has the similar rotational symmetry shown in the EDP's of the QCs. In this case, it can be concluded that unclear HREM images of QCs may imply that the corresponding QCs are perturbed nonclassical crystals. We prefer the second interpretation on QCs since it agrees with the widely held assumption of solid state physics. Consequently, the key point of the arguments about the nature of QCs is whether QCs are essentially aperiodic structures or periodic ones. This may be concluded to judge whether EDP's of QC's have strict 5-, 8-, 10, and 12-fold symmetries and recognize whether HREM's of QCs have the characteristics of periodic structures. Therefore we need to develop a new theory to describe nonclassical periodic lattices; we need to propose effective methods of digital image processing to analyze EDP's and HREM images of QCs. In this paper, we will review these topics studied by our research group, including some new achievements.

The outline of the present paper is as follows. Section 2 collects some new theory and methods of digital image processing. Section 3 deals with and analyses some EDPs and HREM images of QCs. Section 4 summarizes this paper.

1 Theory and Methods

In this section, we will briefly introduce the nonclassical crystallographic groups (NCGs) (see references [33 ~ 36] for detail), the algorithm to determine the center position of diffraction spots in EDP[37], and the algorithm to process HREM images[38,39].

1.1 Nonclassical crystallographic groups

The purpose to set up NCG is to describe nonclassical periodic lattices. Consequently the concept of the product operation on translations and rotations introduced by the classical crystallographic group (CCG) needs to be generalized.

Let T_1 and T_2 be translation mapping with different directions from the plane R^2 onto R^2 and $R_{2\pi/n}$: $R^2 \to R^2$ be rotation mapping through an angle $2\pi/n$ about a given n-fold center O of rotation. Then $\{T_1, T_2, R_{2\pi/n}\}$ generate a group with respect to the mapping composition operation $*$. The CCG theory claims that if all element of the group acting with O generates a periodic lattice, then the lattice only allows 2-, 3-, 4-, or 6-fold centers of the rotation.

Let G_1 be a group produced by $R_{2\pi/n}$ under the operation $*$, and G_2 be a group generated by T_1 and T_2 with respect to the operation $*$. Denote $G = G_1 \times G_2 = \{(R, T): R \in G_1, T \in G_2\}$. The product operation $\bullet$ on G is a rule combining two elements of G such that for any element (R_1, T_1), $(R_2, T_2) \in G$, $(R_1, T_1) \bullet (R_2, T_2) = (R_1 * R_2, T_1 * T_2)$. Then G is a commutative group called an NCG.

Define any element $(R, T) \in G$ as a mapping from R^2 onto R^2 such that for any point P in R^2, $(R, T)P = T * RP$. Let P be a point which is not equivalent to the rotation center O. Then the lattice point set $L = \{(R, T)O, (R, T)P: (R, T) \in G\}$ is called a nonclassical crystallographic lattice (NCL). $\{O, P\}$ is called a generating set. An NCL allows any kind of rotations and, in particular, the centers of locally 5-, 8-, 10-, or 12-fold rotational symmetries, which cannot be generated via CCGs.

Let β be the angle between two straight lines along the translations T_1, T_2 directions, and d_1 and d_2 the translation distances of T_1 and T_2, respectively. Then an NCG can be denoted by $G = G(2\pi / n, \beta, d_1, d_2)$. A complex NCL can be described via so-called direct sum of NCGs. The three kinds of NCLs are shown in Fig. 1.1 (let the line-linked regular polygons have radius b). These lattices belong, respectively, to direct sum groups:

$G(2\pi/8, \pi/2, d_1, d_2) \oplus G(2\pi/8, \pi/2, d_1, d_2)$ where $d_1 = d_2 = 2a\cos(\pi/4)$,

$G(2\pi/12, \pi/3, d_1, d_2) \oplus G(2\pi/12, \pi/3, d_1, d_2)$ where $d_1 = d_2 = 2a\cos(\pi/12)$, and

$G(2\pi/10, 2\pi/5, d_1, d_2) \oplus G(2\pi/10, 2\pi/5, d_1, d_2)$

$\oplus G(2\pi/10, 2\pi/5, d_1, d_2)$

where $d_1 = d_2 = 2a\cos(\pi/5)$.

The positions of the "diffraction spots" (strong diffraction spots in the case of Figs. 1.1(a), (c)) and the distances between two neighboring diffraction spots on the first three "concentric circles" in the FTP's (see Figs. 5(a,c) in [33], and Fig. 3.3(b) in [34]) of the lattices given in Figs. 1.1(a ~ c) are shown in Figs. 1.2(a ~ c), respectively. These graphs illustrate that very simple nonclassical periodic lattices can generate almost perfect 8-, 10- and 12-fold rotational symmetries. The apparent differences of the distances only occur on the innerest

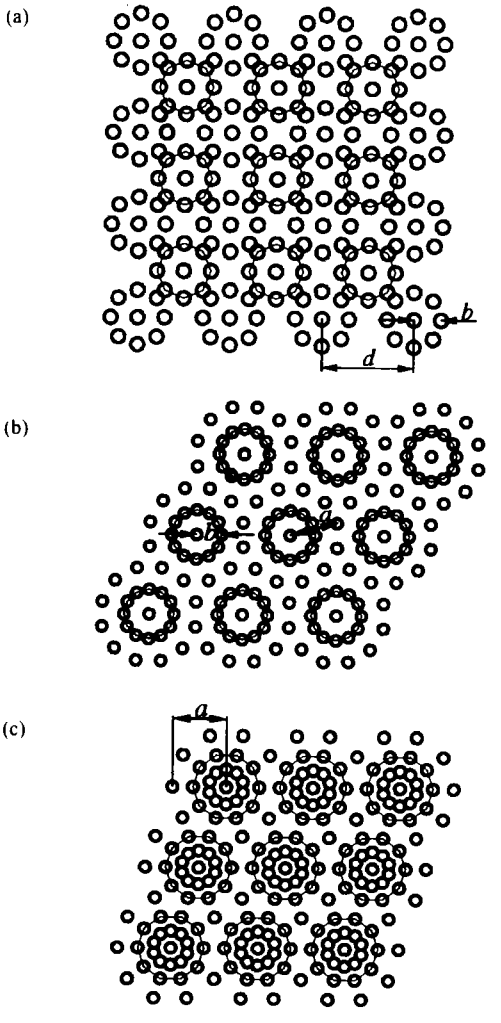

Fig. 1.1 Nonclassical periodic lattices

(a) with locally 8-fold symmetry where $b = a(\sqrt{2} - 1)$, $d = 2a\cos(\pi/4)$ is the translation distance;

(b) with locally 12-fold symmetry where $b = 2a\sin(\pi/12)$;

(c) with locally 10-fold symmetry where $b = a(\sqrt{5} - 1)/2$ $c = a\sqrt{(5 - 2\sqrt{5})} / 5$ is the radius of the smallest

"concentric circles". In the case of the QCs with 5-, 8-, or 10-fold rotational symmetries, the diffraction spots at the origins are often too big so that the diffraction dots on the innerest "concentric circles" cannot be distinguishable from the spots at the origins.

1.2 Algorithms for recogniting EDP's

The diameter of a bright spot in the EDP of a periodic structure is proportional to the corresponding diffraction intensity $|I(h,k,l)|^2$ where $I(h, k, l)$ is the Fourier transform of the structure at the reciprocal-lattice point $ha_1^* + ka_2^* + la_3^*$. It ca be assumed that an ideal diffraction spot is a circle. We name it "diffraction circle".

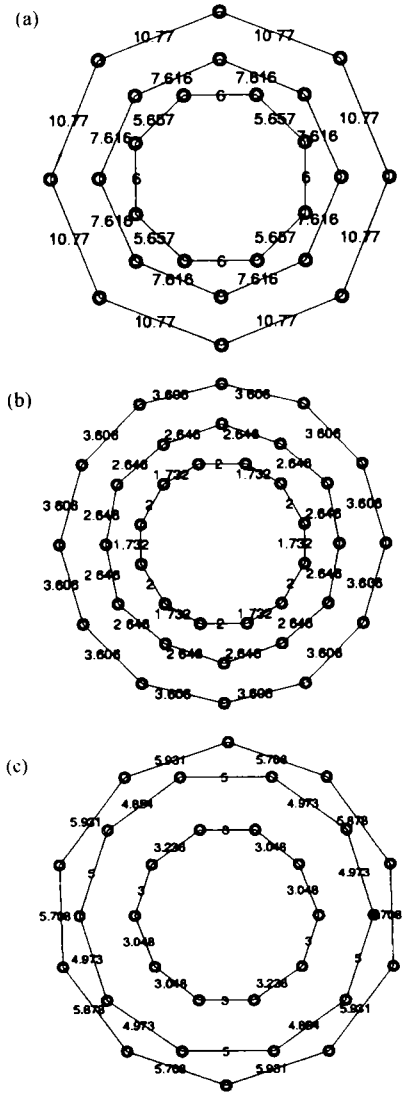

Fig. 1.2 The positions of the "diffraction spots" and the distances between two neighboring diffraction spots on the "concentric circles" in the FTP's of the periodic lattices. (a) with locally 8-fold rotational symmetry; (b) with locally 12-fold rotational symmetry; (c) with locally 10-fold rotational symmetry

Hereafter, it is assumed that an EDP photograph is measured by using a scanner. Hence the corresponding image x and y axes are quantized into square picture elements, pixels. Numerical values are assigned to image grey level. The resulting picture function at the (i, j)th pixel (ith row, jth column) is denoted as $f(i, j)$. Every value $f(i, j)$ is an integer and $1 \le f(i, j) \le 255$. Therefore, the grey level $f(i, j)$ is proportional to the diffraction intensity at the corresponding position in the EDP.

It is assume that a digitized image is a 2-dimensional discrete random field which is a collection of random variables. Each random variable is supposed to have a Gaussian distribution, representing the brightness at the pixel of the image. Consequently, the Gaussian noise makes the image of an ideal diffraction circle become a perturbed circle-like object.

The radius of every diffraction circle can be determined based on a pre-assigned grey level g. This means that the boundary points of every diffraction circle consist of the pixels with grey level g. Therefore the center of a diffraction circle can be found via it's boundary points. The pre-assigned grey level g is called the radius grey level. However perturbation of image prevents the accuracy of the determination of the center position of diffraction spots. It is desirable that an algorithm could restore the circle-like object to an exact circle.

Unfortunately, such a reconstruction algorithm does not exist in general image processing circumstances[40]. However, the following approache seems successfully to have recognized centers of diffraction circles in their perturbed images.

Definition 1.1 For a $(2n+1) \times (2n+1)$ filtering window (also see Def. 3.1 in [37], Def. 1 in [38] and [39]) and a given radius grey level g, the accepting rule is a criterion such that if $(2n^2 + 2n + 1)$ or more pixels in the window have the grey values which are larger than g, then the center of the window will be classified to the class consisting of the diffraction circles in the corresponding image. Otherwise the center will be considered not to belong to any diffraction circles.

Definition 1.2 Let N be the non-negative

integer set and $G \subset N^3$ the image of an EDP generated via a scanner. For a given grey level g and a $(2n+1) \times (2n+1)$ filtering window, the recognizing operator S is a mapping from G to N^3 such that for any element $(i, j, f(i, j)) \in G$, $S((i, j, f(i, j))) = (i, j, \lambda(i, j))$ where $\lambda(i, j) = g$ if according to the accepting rule (i, j) belongs to a diffraction circle otherwise $\lambda(i, j) = 0$.

If there is a positive integer m such that $S^{m+l}(G) \equiv S^m(G)$, $l = 0, 1, 2, \cdots$, then $S^m(G)$ is called a stationary image.

Algorithm A Let a digitized circle with additive Gaussian noise occupy m rows and n columns. In the ith row, the x coordinates of the circle have the forms: m_{1i}, $m_{1i}+1$, $\cdots$, $0, \cdots$, $m_{2i}-1$, m_{2i}, $i = 1, 2, \cdots$, m where m_{1i}'s and m_{2i}'s are integers. In the j th column, the y coordinates of the circle have the forms: n_{1j}, $n_{1j}+1$, $\cdots$, 0, $\cdots$, $n_{2j}-1$, n_{2j}, $j = 1$, 2, $\cdots$, n where n_{1j}'s and n_{2j}'s are also integers. Then the coordinate of the center of the circle is determined by the formulas

$$\bar{X} = \frac{1}{m}\sum_{i=1}^{m}\frac{m_{1i}+m_{2i}}{2}, \quad \bar{Y} = \frac{1}{n}\sum_{j=1}^{n}\frac{n_{1j}+n_{2j}}{2}.$$

Using 3×3 window recognizing operators processes the ideal quantized circle (Fig. 1.3(a)) with additive Gaussian noise shown in Fig. 1.3.(c). After 19 time iterating, a stationary images is obtained. Table 1.1 gives the calculated centers via Algorithms A. The accurate center of the ideal quantized circle is (100, 100). Consequently, the algorithm has efficiently recognized the correct center of the perturbed digitized circle. Although the center listed in the second row seems to be equally well to the data processed via the window recognizing operators, there are in fact many "quasicenters" determined wrongly from Fig. 1.3(d). This means that it is necessary to use the recognizing operators to pre-process images. The table also illustrates that we can get the center coordinate with an accuracy of 1 pixel only after dealing with Fig. 1.3(d) for one time via the recognizing operators.

1.3 HREM image processing

Convexity is a fundamental characteristic of bright specks in many HREM images of matters. It has been found that so-called smooth operator can efficiently reduce noise and recover convexity of bright specks in HREM images which is defined via the following (also see [38, 39]).

Table 1.1 Calculated center coordinates (pixels) of the (perturbed) diffraction circles

Circles shown in	Algorithm A
Fig.1.3(b)	(100, 100)
Fig.1.3(d)	(101.1, 100.1)
Fig.1.3(e)	(101.1, 99.9)
Fig.1.3(f)	(100.7, 99.9)

Definition 1.3 For a $(2l+1) \times (2l+1)$ filtering window, let G be a digitized image. The smooth operaor S_{2l+1} is a mapping from $G \subset N^3$ to N^3 such that for any $(i, j, f(i, j)) \in G$

$$S_{2l+1}: (i, j, f(i, j)) \to (i, j, \text{mean}\{\text{the largest } 2l^2+2l+1 \text{ numbers in set } g(i, j)\})$$

where $g(i, j) = \{\tilde{f}(h, k): h = i-l, i-l+1, \cdots, i+l; k = j-l, j-l+1, \cdots, j+l, \text{ and}$

$$\tilde{f}(i, j) = \begin{cases} f(i,j) & \text{for } (i, j) \in G \cap N^2, \\ 0 & \text{otherwise.} \end{cases}$$

$S_{2l+1}(G)$ is called the first smooth image of G. For a positive integer m, $S^m_{2l+1}(G)$ is called the mth smooth image of G.

The HREM image of the Al-Mn-Si icosahedral QC with the incident beam along the 2-fold symmetry axis[41] is digitized with an accuracy of 600 dpi by using a Screen DT-S1030 AL scanner (Fig. 1.4(a)). The digitized image G is processed via using a S_3 smooth operator acts G for 4 times. The 4th smooth image $S_3^4(G)$ is given in Fig. 1.4(b). The periodic characteristics can be recognized from Fig. 1.4(b). This QC can be understood to consist of huge unit cells[39].

2 Applications

In this section, we give the applications of the theory and the methods introduced in the previous section to the studies of the EDP's of some QCs. The results show that the QCs with 5-, 8-, 10-, and 12-fold symmetries can be understood to be generated by complex nonclassical perturbed periodic structures.

2.1 Analysis for the EDP of $Mn_{82}Si_3Al_{15}$ QC

The discovery of the Cr-Ni-Si and V-Ni-Si with octagonal symmetric EDP's was reported by Wang, Chen, and Kou in 1987[4]. Later, more perfect octagonal phase which gives a much

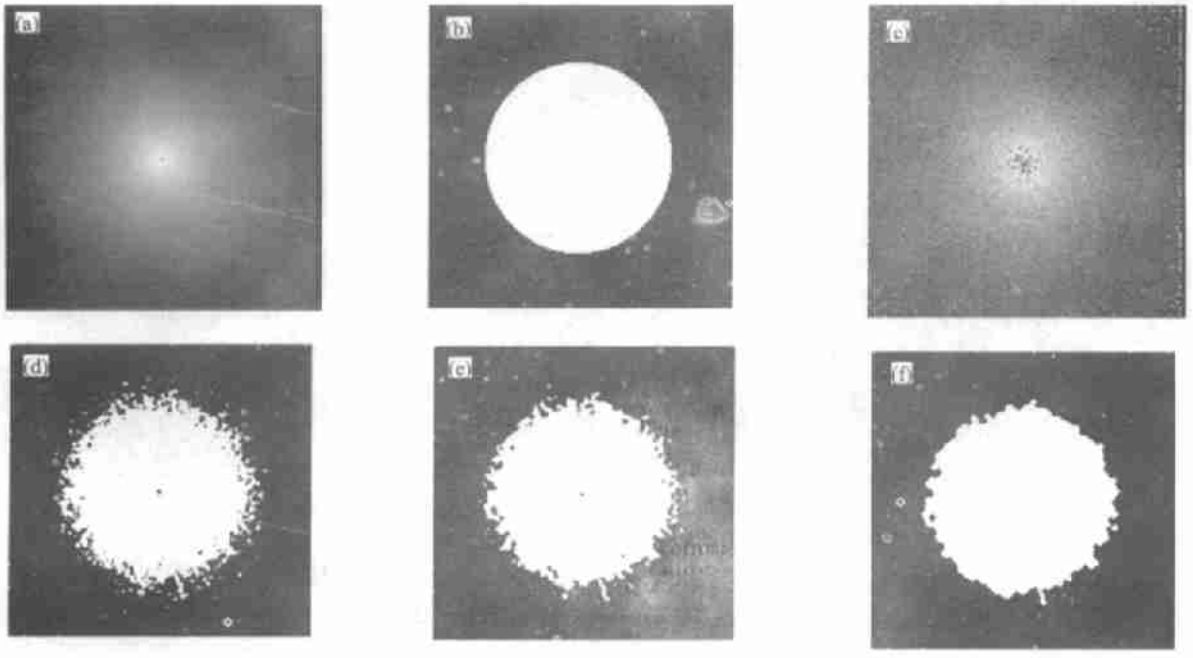

Fig. 1.3 (a) An ideal quantized diffraction circle with center (100, 100); (b) its two-valued image taking radius grey level 100; (c) The ideal diffraction circle is disturbed by the additive Gaussian noise with mean 0 and varian 20, and (d) its two-valued image taking radius grey level 100. The circle shown in (d) is processed via the 3 × 3 window recognizing operator for one time (e), and for 19 times (f) which becomes a stationary image

sharper EDP displaying "apparent" 8-fold symmetry was found by Wang, Fung and Kou in a rapidly solidified $Mn_{82}Si_3Al_{15}$ alloy[42].

The popular beliefs are that these octagonal phases can be interpreted as two-dimensional aper-iodic structures[4,42,43]. However the periodic tiling shown in Fig. 1.1(a) has also almost perfect 8-fold rotational symmetric FTP (see Fig. 1.2(a)).

The EDP observed in the $Mn_{82}Si_3Al_{15}$ Phase (see reference [42]) seems to show "apparent" 8-fold rotational symmetry. However, the precise determination of the positions of the diffraction spots shows that the positions of the diffraction spots apparently deviate from the 8-fold symmetry.

For this purpose, the original photograph of the EDP of the $Mn_{82}Si_3Al_{15}$ alloy is taken from Wang's Ph. D Thesis (see Fig. 4.1.2 in reference [43]) and is measured with an accuracy of 3 000 dpi by using a Screen DT-S1030 AI scanner. A digitized image of the EDP is given in Fig. 2.1(a). In the digitized image, first take the radius grey level $g = 120$, and then use a 3 × 3 filtering window smooth operator S to process the image for one time, after that determine the centers of

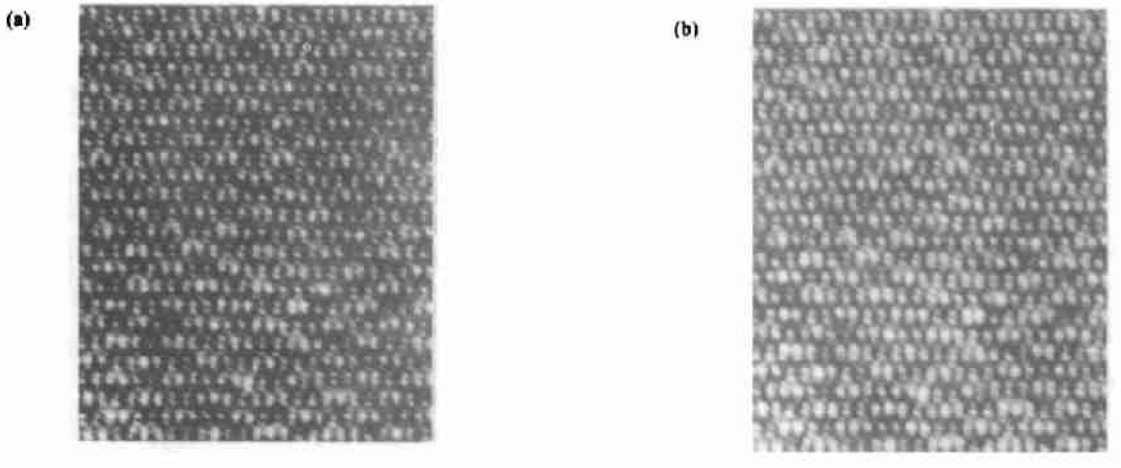

Fig. 1.4(a) The digitized HREM image of Mn-Al-Si icosahedral quasicrystal with the incident beam along the two-fold symmetry axis, and (b) its 4th smooth image (Courtesy of K. Hiraga, Tohoku University)

the diffraction circles in the processed image via algorithm *A*.

The calculated coordinate centers of the diffraction circles are shown in Fig. 2.1(b). It can be found that the deviation of the coordinate centers cannot be interpreted via Fig. 1.2(a). Careful examination and analysis show that these center positions can be indexed by an $h-k$ orthogonal coordinate system, and the ratios of the unit lengths of the h axis and the k axis are $\sqrt{2}$. The corresponding positions are (0, ± 10), (0, ± 14), (± 2, ± 7), (± 5, ± 3), (± 5, ± 7), (± 7, 0), (± 7, ± 10), and (± 10, 0) shown in Fig. 2.2(a). If increasing 60.3 in scale, then the multiplied graph of Fig. 2.2(a) is shown in Fig. 2.2(b).

The tiling given in Fig. 2.3(a) has locally 8-fold rotational symmetry, which can be described by the direct sums of 6 NCG $G(2\pi/8,\ \pi/2,\ 2a\cos(\pi/8),\ 4a\cos(\pi/8)\cos(\pi/4))$s. In Fig. 2.3(a), if let the atoms in the gaps have scattering factor 2, and the atoms on the circles with radius b or at the centers of the octagons have scattering factor 1, and the atoms on the circles with radius c have scattering factor 0.5, then the FTP of the tiling is given in Fig. 2.3(b).

The positions of the centers of the strong diffraction spots on the first three "concentric circles" are exactly the same as those shown in Fig. 2.2(a) which are very close to the ones given in Fig. 2.1(b).

Furthermore, along the horizontal direction in Fig. 2.1(a), the ratios of two successive distance from the origin of the first five diffraction spots calculated by algorithm *A* are 1.45, 1.39, 1.22, 1.40; along the vertical direction in Fig. 2.1(a), the ratio of two successive distance from the origin of the first five diffraction spots determined via algorithm *A* are 1.41, 1.42, 1.20, 1.41. On the other hand, along the h axis direction (see Fig. 2.3(b)), the ratios of two successive distance from the origin of the first five strong diffraction spots are $10/7 \approx 1.43$, $14/10 = 1.4$, $17/14 \approx 1.21$, $24/17 \approx 1.41$; along the k axis direction (see Fig. 2.3(b)), the ratios of two successive distance from the origin of the first five strong spots are $14/10 = 1.4$, $20/14 \approx 1.429$, $24/20 = 1.2$, $34/24 \approx 1.416$. Comparing the data of the experimental EDP with the ones of the

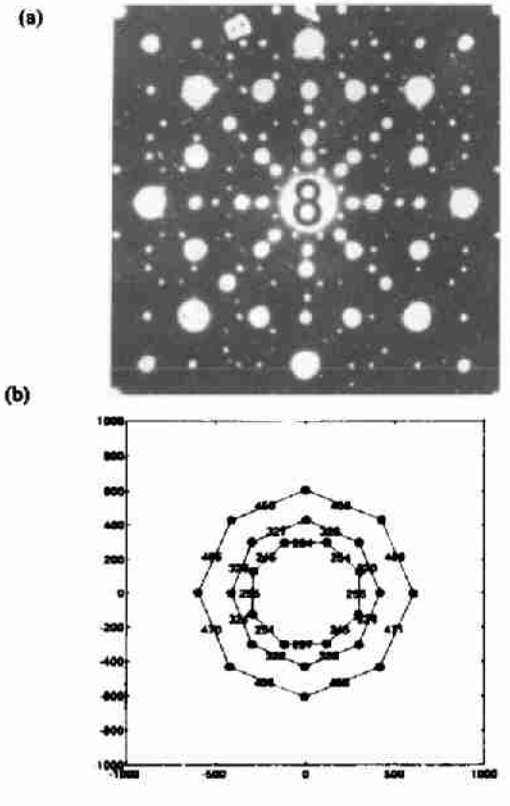

Fig. 2.1 (a) The digitized EDP of Mn-Al-Si quasicrystal with 8-fold symmetry; (b) the calculated coordinates of the centers of the strong diffraction spots on the first three "concentric circles" are indexed by pixels (Courtesy of the Graduate School, USTB)

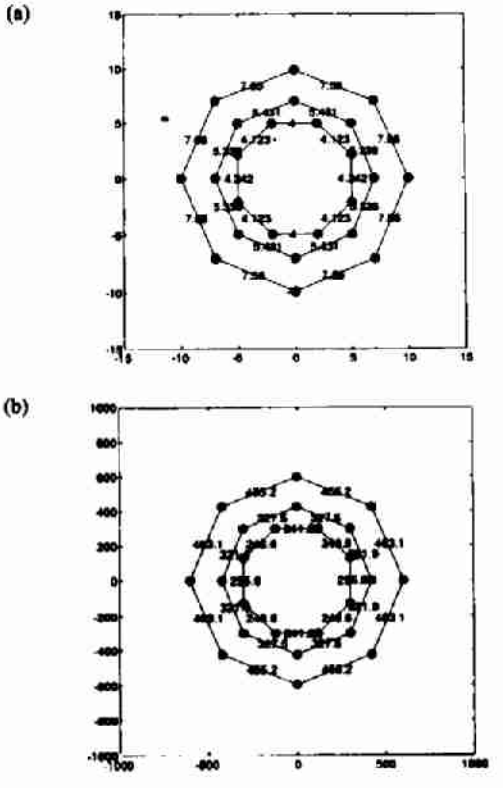

Fig2.2 (a) The coordinates of the lattices with approximate 8-fold symmetry are located at an orthogonal system with different unit lengths; (b) the coordinates are multiplied by a factor 60.3

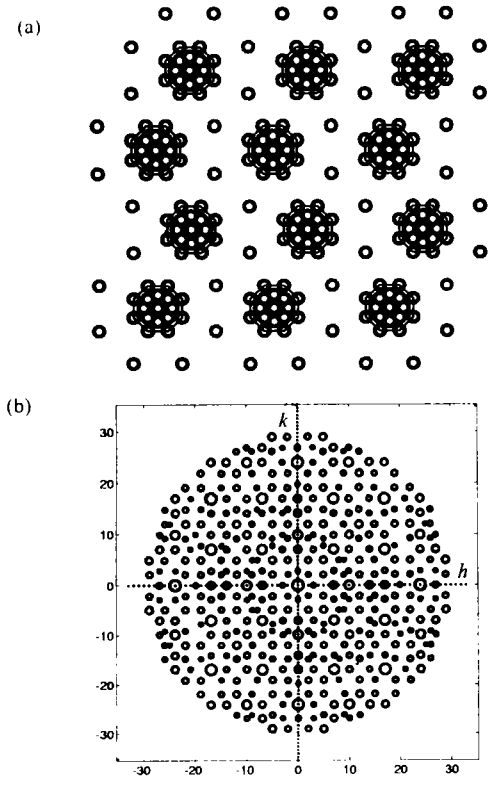

Fig. 2.3 (a) A lattice point set with approximate 8-fold symmetry. In the lattice, let a be the radius of the biggest octangons, $b = a(\sqrt{2} - 1)$ the radius of the line-linkedones, and $c = b\sqrt{(2 - 2\sqrt{2}) / 2}$ the radius of the smallest ones; (b) FTP of the lattice

FTP of the periodic model, we can conclude that an orthorhombic crystal model can explain the 8-fold symmetry displaying in the EDP of the experimental $Mn_{82}Si_3Al_{15}$ alloy although the "model" in Fig.2.3(a) fails to generate FTP's which are similar to all corresponding EDP's of the MnSiAl QC along other diffraction directions, respectively (See Fig.4.1.2 in [43]).

2.2 Analysis for the EDP's of QCs with 10-fold symmetry

The original photographs of the EDP's of the $(Al_6Fe)_{98}B_2$ and Al-Cu-Co-Ge[44] QC's with 10-fold rotational symmetries (see Figs. 2.4(a) and 2.5(a)) are scanned with accuracies of 5 000 dpi and 3 000 dpi by using a Screen DT-S1030 AI scanner, respectively.

For the quantized (Al-Fe)B image, take the corresponding radius grey level $g = 120$. And for the digitized Al-Cu-Co-Ge image, take $g = 187$. Then use a 3×3 window recognize operator to process the two images for one time and 5 times, respectively. After that use algorithm A to calculated the coordinates of the center positions of the spots (strong spots in the image of (Al-Fe)B) on the first three "concentric circles" in the two images. The results are schematically presented in Figs. 2.4(b) and 2.5(b), which apparently deviate from corresponding strict 10-fold rotational symmetries.

If Fig. 2.4(a) is an image of a perturbed strictly symmetric pattern. The average value of the distances between the "symmetric points" on every "concentric circle" should be taken as the diameter of the corresponding concentric circle of the symmetric pattern. And 10 spots should be distributed homogeneously on the corresponding concentric circles. We call such a pattern as symmetric pattern. Based on the calculated data of the center positions of the EDP of the (Al-Fe)B QC, the corresponding symmetric pattern is shown in Fig. 2.6. Clearly, Fig. 2.4(b) should be explained as perturbation of a pattern located at integral lattice points in a corresponding orthogonal or oblique coordinate system rather than the perturbation of the pattern given in Fig. 2.6.

In Reference [45], we proposed a periodic atomic model to interpret the Al-Fe QC with 10-fold rotational symmetry[7]. The center positions of the spots in the FTP of that model which are corresponding to the center positions in Fig. 2.5(b) are shown in Figs.2.7(a) and 2.7(b). On the other hand, the average diameters of the "concentric circles" in Fig. 2.5(b) are $D_1 = 930.1$, $D_2 = 1\,548.7$, and $D_3 = 2\,480.5$. If Fig. 2.5(b) represents a perturbed FTP of a Penrose tiling, then the corresponding diameters of the concentric circles in the FTP of the Penrose tiling might be $D_{p1} = D_2(\sqrt{5} - 1)/2$, $D_{p2} = D_2$, and $D_{p3} = D_2(\sqrt{5} + 1)/2$. Therefore the center positions of the spots in the FTP of the Penrose tiling can be described via Fig. 2.8.

Now let us investigate whether the observed positions of the experimental spots are closer the positions of the periodic model (Fig. 2.7(b)) or those of the Penrose model (Fig. 2.8). For $i = 1, 2, \cdots, 30$, let (x_e^i, y_e^i), (x_s^i, y_s^i), and (x_p^i, y_p^i) be the coordinates of the experimental diffraction spots, the dots of the periodic model, and the spots of the Penrose model, respectively. The deviation parameters are defined by the following formulas:

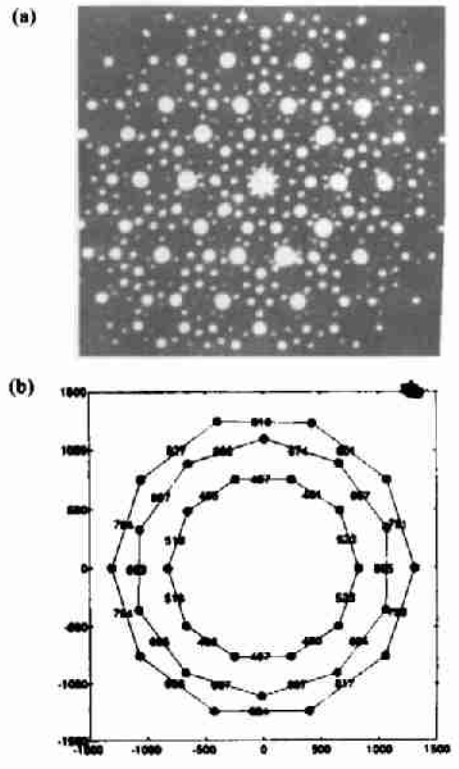

Fig. 2.4 (a) The digitized EDP of (Al-Fe) B quasicrystal with 10-fold symmetry, and (b) the calculated coordinates of the centers of the strong diffraction spots on the first three "concentric circles" are indexed by pixels (Courtesy of Zhou Yuqing, Institute of Physics, Chinese Academy of Sciences)

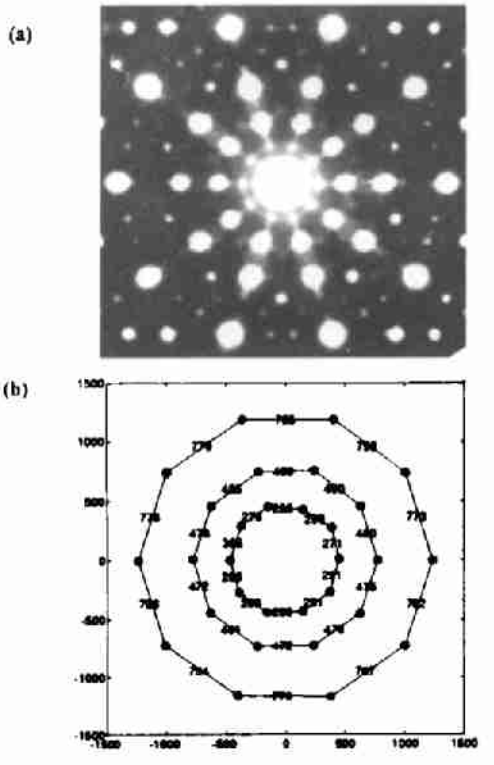

Fig. 2.5 (a) The digitized EDP of Al-Cu-Co-Ge quasicrystal with 10-fold symmetry, and (b) the calculated coordinates of the centers of the strong diffraction spots on the first three "concentric circles" are indexed by pixels (Courtesy of Chen Lifan, Institute of Physics, Chinese Academy of Sciences)

$$D_{cp} = \left[\sum_{i=1}^{30} \{(x_c^i - x_p^i)^2 + (y_c^i - y_p^i)^2\} \right]^{1/2}, \quad (1)$$

$$D_{cs} = \left[\sum_{i=1}^{30} \{(x_c^i - x_s^i)^2 + (y_c^i - y_s^i)^2\} \right]^{1/2}, \quad (2)$$

$$D_{sp} = \left[\sum_{i=1}^{30} \{(x_s^i - x_p^i)^2 + (y_s^i - y_p^i)^2\} \right]^{1/2}. \quad (3)$$

The calculated results are summarized in table 2.1. The means of the different deviations are given in the second row. The corresponding maximum deviations and minimum deviations are included in the 3th row and the 4th row, respectively.

From table 2.1, we can conclude that the positions of the spots of the periodic model and the positions of the spots of the Penrose model have the same "order" deviation from the experimental data. However, Fig. 2.5(b) suggests that it might be understood as a perturbed image whose lattice points are located at integer coordinates in an orthogonal or an oblique coordinate system.

2.3 Analysis for EDP's of 5-fold QCs

Now let us study the EDP's of the other QCs with 5-fold symmetries. The original photographs of the EDP's of the $Al_{80}Mn_{20}$ QC[46] and the Al-Mn QC were scanned with accuracies of 5 000 dpi and 3 000 dpi by using a Screen DT-S1030 AI scanner,

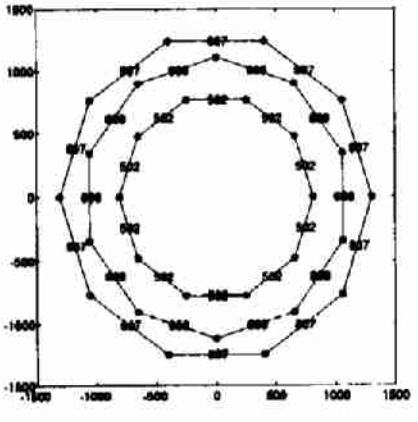

Fig. 2.6 A symmetric pattern is set up via the calculated data of the center positions of the EDP of the (Al-Fe) B image

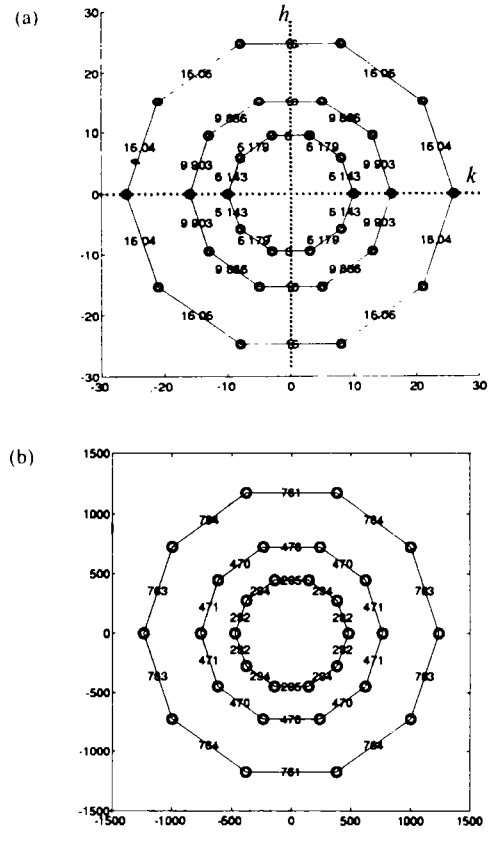

Fig. 2.7 (a) The positions of the "diffraction spots" in the FTP of the model given in reference [45]; (b) multiplied by a factor 47.55

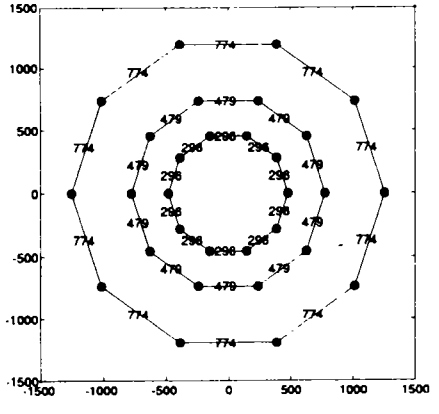

Fig. 2.8 The center positions of the spots in the FTP of a Penrose Model

respectively. For the quantized $Al_{80}Mn_{20}$ image, take the corresponding radius grey levels $g = 60$. And for the digitized Al-Mn image, take $g = 150$. Then use a 3×3 filtering window smooth operator to process the two images for one time and 2 times, respectively. After that use algorithm A to calculated the coordinates of the center positions of the "strong" spots on the first three "concentric circles" in the two images. The calculated center positions are shown in Fig. 2.9(b) and 2.10(b), respectively.

The pattern in Fig. 2.10 apparently deviates from the strict sense symmetry. However, the deviation of the center positions in Fig. 2.9 is not obvious, and the average diameters of the first three "concentric circles" are $D_1 = 950.5$, $D_2 = 1\,546.7$, and $D_3 = 2\,506.4$. Now let us take the points on the three "concentric circles" in Fig. 5 in reference [45] as those shown in Fig. 2.11(a), then increase the scalar of the pattern by 29.6 (see Fig. 2.11(b)). On the other hand by the reasons stated in the last section, the diameters of the three concentric circles of the corresponding Penrose model might be taken as $D_{p1} = (\sqrt{5} - 1)D_2/2$, $D_{p2} = D_2$, and $D_{p3} = (\sqrt{5} + 1)D_2/2$, whose pattern is given in Fig. 2.12.

Table 2.1 Position deviations between experimental phase, periodic model, and Penrose model

	D_{es}	D_{ep}	D_{sp}
Deviation	426.9	467.2	374.1
Mean	14.2	15.6	12.5
Maximum	31.4	33.4	19.1
Minimum	0.1	1.7	3.1

By formulas (1) ~ (3), the deviation parameters of the two pattern with the experimental data are given in Table 2.2. This table illustrates that the periodic pattern and the Penrose Pattern are too similar to be distinguishable. And they both have the same "order" deviation from the experimental data.

Remark 2.1 The processed HREM images of the Al-Mn-Si with 5-fold rotational symmetry show obviously periodic characteristics (see Fig. 1(b) in [38], Fig. 1(b) in [39], and Fig. 1.4(b)). The FTP of a periodic model presented based on these HREM images is given in Fig. 1(c) in reference [39]. The center positions of the strong diffraction spots on the first three "concentric circles" in the FTP are shown in Fig. 2.13. However, the determinations of the positions of the diffraction spots show that none of the EDPs shown in subsections 2.2 and 2.3 can be interpreted via this pattern.

Remark 2.2 The qualities of the photographs of EDP's might affect the accuracies of the determinations of the center positions of diffraction spots. Figs. 2.14(a) and 2.14(b) are two binary-valued mages of the EDP's of the Mn-Al QC (Fig. 2.9(a))

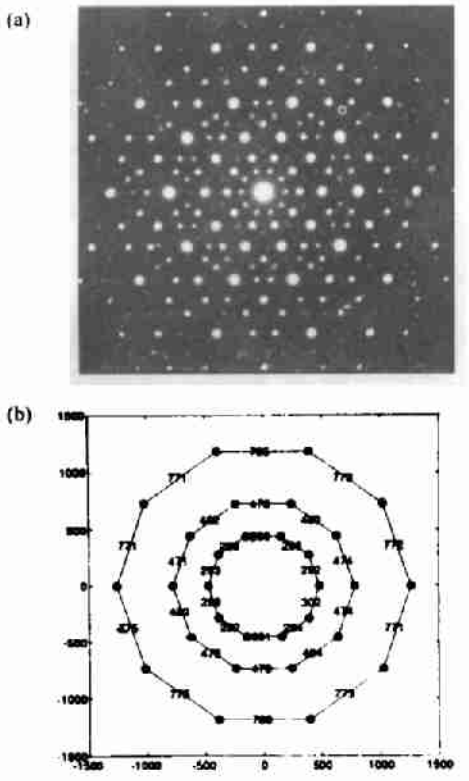

Fig. 2.9 (a) The digitized EDP of $Al_{80}Mn_{20}$ quasicrystal with 5-fold symmetry; (b) the calculated coordinates of the centers of the strong diffraction spots on the first three "concentric circles" are indexed by pixels (Courtesy of Miao Biahe, USTB)

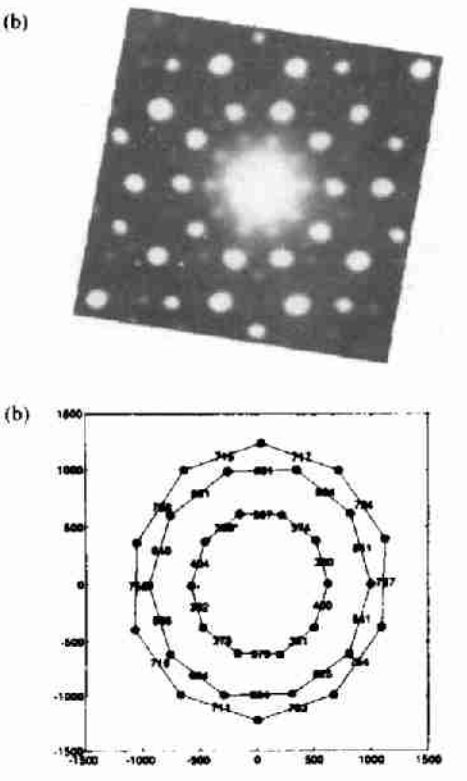

Fig. 2.10 (a) The digitized EDP of Al-Mn quasicrystal with 5-fold symmetry; (b) the calculated coordinates of the centers of the strong diffraction spots on the first three "concentric circles" are indexed by pixels (Courtesy of Zhou Yuqing, Institute of Physics, Chinese Academy of Sciences)

and the Al-Cu-Co-Ge QC (Fig. 2.5(a)), respectively. Clearly, the quality of the EDP of the Al-Cu-Co-Ge is less than the one of the Mn-Al which might explain why the symmetry is so bad in Fig. 2.5(b).

2.4 Atomic model for 12-fold QC

The QC with 12-fold symmetric EDP was firstly reported by Ishimasa, Nissen, and Fukano in Ni-Cr alloy[8]. Clearer EDP's with the same symmetry but showing different features were observed by Chen, Li, and Kuo in V-Ni and V-Ni-Si phases[9]. It has been pointed that the center positions of the diffraction spots in these EDP's obviously deviate from the corresponding strict sense 12-fold symmetries and can be indexed by two orthogonal coordinate systems (see Fig. 1 in [32], Fig. 1 in [30], Fig. 1

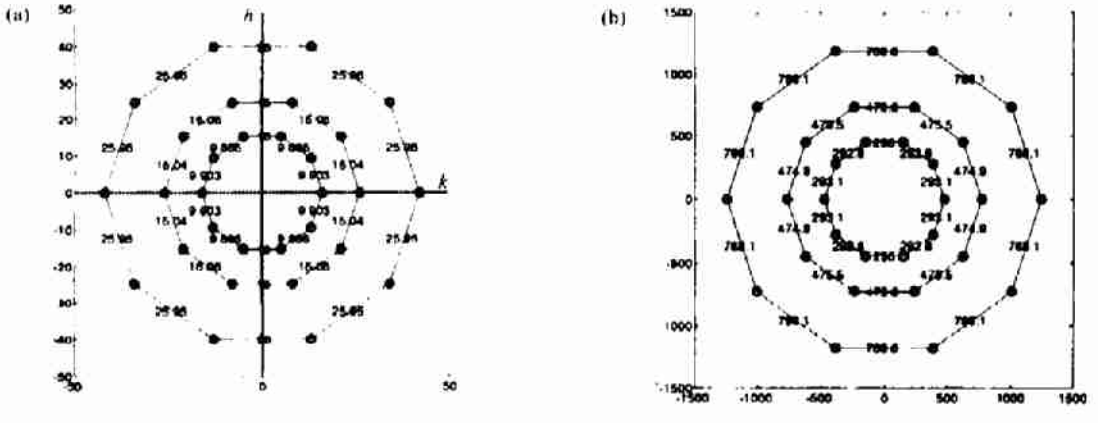

Fig. 2.11 (a) The center positions on the three "concentric circles" in the FTP given in refercence [45]; (b) multiplied by a factor 29.6

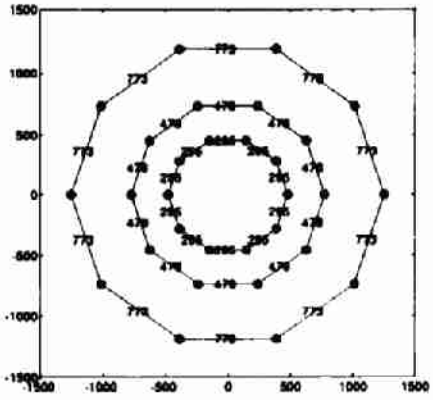

Fig.2.12 The center positions of spots in the FPT of a Penrose model

Table 2.2 Position deviations between experimental phase, periodic model and Penrose model

	D_{es}	D_{ep}	D_{sp}
Deviation	192.1	210.7	37.7
Mean	6.6	7	1.3
Maximum	13.3	12.8	2.1
Minimum	1.6	1.3	0.2

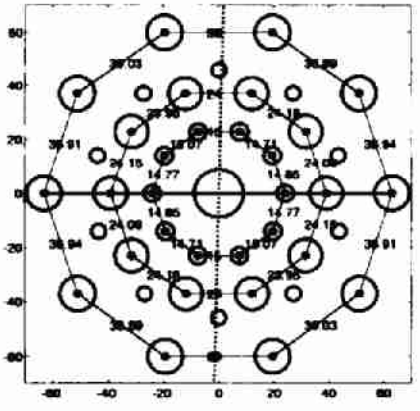

Fig.2.13 The FTP of the periodic model of the Al-Mn-Si QC

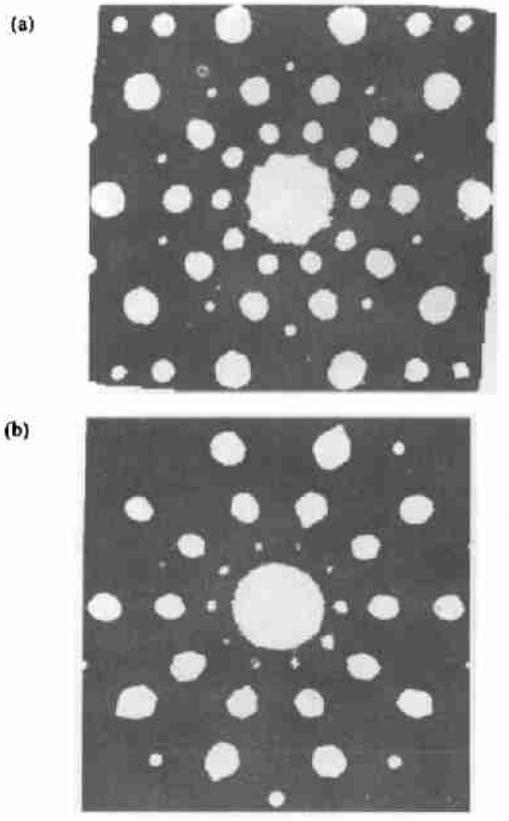

Fig.2.14 (a) The binary image of the EDP of the Mn-Al QC taken radius grey level as 60; (b) The binary image of the EDP of the Al-Cu-Co-Ge taken radius grey level as 187. If the radius grey level is less than 187, the diffraction spots on the first "concentric circles" will be not distinguishable from the one at the origin

in [31], respectively). The center positions of the diffraction spots on the first three "concentric circles" are shown in Figs.2.15(a) and 2.15(b).

A periodic atomic model has been proposed to interpret the V-Ni 12-fold QC[32]. The unit cell of

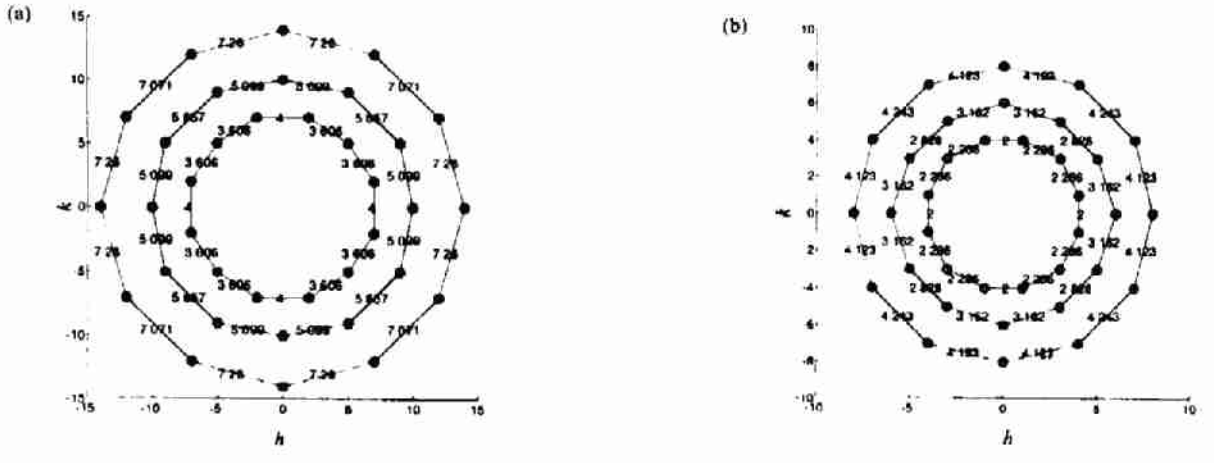

Fig. 2.15 The positions of the diffraction peaks of the QCs with 12-fold rotational symmetries can be indexed via two orthogonal coordinate systems (a) Ni-Cr phase; (b) V-Ni alloy

the model consists of two kinds of so-called T-polyhedron columns shown in Fig. 2.16 where white balls represent atom V and the black ones represent atom Ni. The projection of the unit cell is given in Fig. 2.17. Let a be the radius of the big dodecagons in Fig. 2.17, and $b = 2a\sin(\pi/12)$ the small ones. The three primitive lattice vectors a_1, a_2, and a_3 can be written as $a_1 = (4a\cos(\pi/12), 0, 0)$, $a_2 = (0, 4a\cos(\pi/12), 0)$, and $a_3 = (0, 0, 8a\tan\theta)$ where $\theta = (\sqrt{6} - \sqrt{2})/4$. There are 160 V atoms and 80 Ni atoms in the unit cell. Further more let the parameter $a = 0.445$ nm. Then the chemical composition of the model is $V_{66.2}Ni_{37.8}$, with a density of $\rho = 7.8 \times 10^3$ kg/m^{-3}. The FTP of the model orthogonal to a "12-fold" axis is shown in Fig. 2.18,

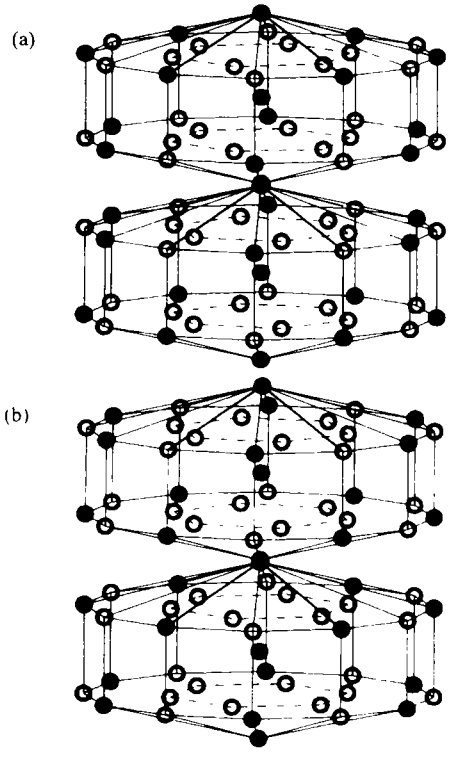

Fig. 2.16 (a) I kind T-polyhedron column; (b) II kind T-polyhedron column

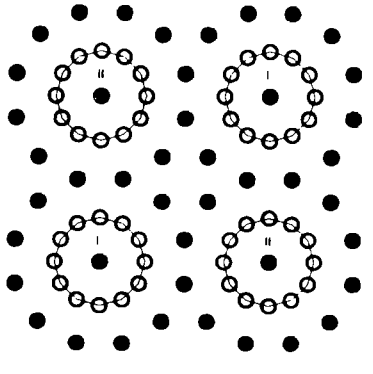

Fig. 2.17 Projection of a unit cell on the x-y plane

the ones along other directions are given in Fig. 4 in reference [32], which are in good agreement with all of the corresponding EDP's of the V-Ni phase. The plane periodic lattice shown in Fig. 2.17 can be described via the direct sum group: $G(2\pi/12, \pi/2, d, d) \oplus G(2\pi/12, \pi/2, d, d)$ where $d = 2a\cos(\pi/12)$.

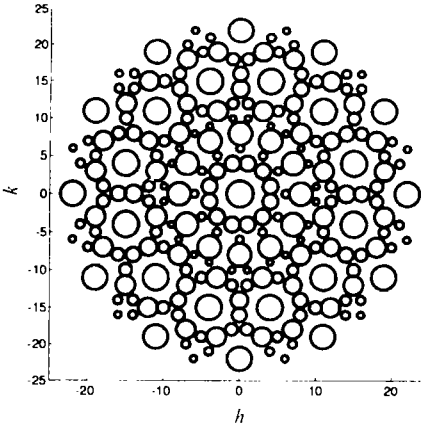

Fig. 2.18 The FTP of the periodic model orthogonal to the "12-fold" axis

3 Concluding Remarks

The NCGs allow any n-fold rotational operations. Theoretically, NCGs can generated infinite kinds of periodic lattices, in particular some very simple nonclassical periodic lattices with locally 8-, 10-, or 12-fold symmetries, whose FTPs have almost perfect 8-, 10-, or 12-fold symmetries, respectively.

Since the formations of EDPs and HREM images of a structure are effected by many unknown factors, it is very difficult to assume their statistical properties – a priori information. Fortunately, one of the key problems for the recognition of EDP's and HREM images is to determine center positions of diffraction spots, which are essentially depends on information of their boundary points with Gaussian noise. Simply algorithms A with the window recognizing operator can efficiently reduce Gaussian noise on boundary points and exactly determine the center positions of perturbed diffraction spots. Another is to recover convexity of perturbed HREM images. The smooth operator has been proved to be a appealing candidate to process HREM images of alloys.

The determinations of the center positions of the diffraction spots of some QCs with 5-, 8-, 10-, or 12-fold rotational symmetries show that the

center positions deviate, more or less, from the corresponding strict sense n-fold rotational symmetries. Even very small deviations can also be understood the perturbations of the FTP's of nonclassical periodic lattices. In particular, two 3-dimensional periodic atomic models and several 2-dimensional nonclassical periodic tilings have been presented to explain the corresponding QCs (also see references [32, 37, 39, 45]).

Processed HREM images of the Al-Mn-Si QC show obviously periodic characteristics (also see reference 38, 39) rather than Penrose tilings. Our recent research on HREM image of Al-Mn QC with 5-fold rotational symmetry[47] shows that the processed HREM image displays another kind periodic characteristic.

All these evidences, although need to be confirmed further, allow us to believe that so-called QCs are essentially (perturbed) nonclassical periodic structures. Consequently, the widely accepted assumption of the solid should not be given up. However the classical crystallographic theory should be generalized. If the NCG had been set up before the discoveries of so-called QCs, more people would have understood the EDP's of QCs were produced by periodic structures.

The applications of the theory and the methods introduced in this paper can be extended to other disciplines. In fact, the image processing approaches have been used to analysis the repeating accuracy of the Sceen DT-S1030 AI scanner. The result shows that the probability of the confidence level of the repeating errors which are less than 2 pixels for calculated center positions of the disturbed diffraction spots is larger than 95%. Another appealing field to use the above image processing methods might be astronomy.

It cannot be concluded that the researches have been complete and conclusive because we need to analyze more and better quantity HREM images and EDP's of QCs, and need to develop more and better theoretic systems and algorithmic tools. However, the tip of the theoretic iceberg has led us to understand, in a new angle, the QC phenomena and microscopic structures, specially when viewed from the broader perspective of ordinary solid matter. As consequences, some uncharted mathematical and physical territories might be systematically explored and exploited for novel applications in the future.

Acknowledgment

The author would like to thank Yin Wanwu and Yu Hanliang for arranging the author to use the research facilities at the USTB, the Beijing Diamond Color Digital Graphic Company Ltd. for discount fee for scanning the EDP's and HREM images, and Yang Zijiang for scanning the phtographs of the QCs.

References

1 Animalu A O E. Intermediate Quantum Theory of Crystalline Solids. New Jersey: Prentice-Hall, Incs, 1977
2 Shechtman D, Blech I, Dratias D, Cahn J M. Phys Rev Lett, 1984, 53: 1951
3 Ye H Q, Wang D N, Kuo K H. Ultra-microscopy, 1985, 16: 273
4 Wang N, Kuo K H. Phys Rev Lett 1987, 59: 1 010
5 Cao W, Ye H Q, Kuo K H. Phys Stat Sol(a), 1988, 107: 511
6 Bendersky L. Phys Rev Lett, 1985, 55: 1 461
7 Fung K K et al. Phys Rev Lett, 1985, 56: 2 060
8 Ishimasa T, Nissen H U, Fukano Y. Phys Rev Lett, 1985, 55: 551
9 Chen H, Li D X, Kuo K H. Phys Rev Lett, 1988, 60: 1 645
10 Penrose R. Bull Inst Math Appl, 1974, 10: 266
11 Mackay A L. Physica, 1982, 114A: 609
12 Levine D, Steinhardt P J. Phys Rev Lett, 1984, 53: 2 477
13 Levine D, Steinhardt P J. Phys Rev 1986, B34: 596
14 Duneau Michel, Katz Andre. Phys RevLett, 1985, 54: 2 688
15 Watanabe Y, Ito M, Soma T. Acta Cryst, 1987, A43: 133
16 Kramer Peter. J Math Phys, 1988, 29: 516
17 Wang Z M, Kuo K H. Acta Cryst, 1988, A44: 857
18 Zhang H, Kuo K H. Phys Rev, 1990-II, B41: 3 482
19 Socolar E S. Phys Rev, 1990-II, B41: 3 482
20 Kuo K H, Feng Y C, Chen H. Phys Rev Lett, 1988, 61: 1 740
21 Teinhart P, Divincenzo D. Quasicrystals: the State of the Art. Singapore: S Word Scientific, 1991
22 Beeli C. J Phys, 1990, 52: 661
23 Jaric M V. Introduction to the Mathematics of Quasicrystals(2). London: Academic Press Inc, 1987
24 Feild R D, Traser H L. Mat Sci Eng, 1984/85(68): L17
25 Pauling L. Nature, 1985, 317:512
26 Pauling L. Proc Natl Acad Sci, USA, 1989, 86: 8 595
27 Pauling L. Proc Natl Acad Sci USA, 1986, 86: 9 637
28 Min Lequan, Li Yi. Journal of Univ of Iron and

Steel Tech Beijing. (in Chinese), 1988, 10(3): 391
29 Ho T L, Li Y H. Phys Rev Lett, 1989, 62: 917
30 Min Lequan, Wu Yuzhen. Phys Rev Lett, 1990, 65: 3 409
31 Min Lequan, Wu Yuzhen. Phys Rev 1992-II, 45: 10 306
32 Min Lequan, Wu Yuzhen. Phys Rev 1994-II, 49: 16 052
33 Min Lequan. Journal of Univ of Sci and Tech Beijing, 1994, 1(2): 104
34 Min Lequan. Advances in Systems Science and Applications, Inauguration Issue, 1995: 52
35 Min Lequan. Journal of Univ of Sci and Tech Beijing, 1996, 3(2): 133
36 Min Lequan. Journal of Univ of Sci and Tech Beijing, 1997, 4(1): 58
37 Zhou Xin, Min Lequan. Systems Analysis Modelling, Simulation 1996, 26: 239
38 Min Lequan, Zhou Xin. Journal of Univ of Sci and Tech Beijing (in Chinese), 1996, 18(3): 299
39 Min Lequan. Journal of Univ of Sci and Tech Beijing 1996, 3(2): 140
40 Harman G T. Image Reconstruction from Projection: the Foundations of Computerized Tomography. New York: Academic Press, 1980
41 Hiraga K, Hirabayyashi M, Inoue A, et al. J Microscopy, 1986, 146: 245
42 Wang N, Fung K K, Kuo K H. Appl Phys Lett, 1988, 52: 2120
43 Wang N. The Discoveries of Eightfold Quasicrystals and Study of Their Corresponding Structures: [dissertation]. Beijing: Univ of Sci and Tech Beijing, 1989
44 Chen L F, Chen H, Li F H. Phil Mag Lett, 1995, 71: 51
45 Min Lequan, Wu Yuzhen. Journal of Unin of Sci and Tech Beijing. 1995, 2(1): 63
46 Miao Baihe, Yang Guobin, Wang Su. Phys Lett, 1987, A121(6): 238
47 Hiraga K, Hirabayyashi M, Inoue A, et al. J Phys Soc Jpn, 1985, 54: 4 077

Appendix

Table 1 Calculated Center Coordinates (pixels) of the (Perturbed) Diffrction Circles of the (Al-Fe)B and Al-Cu-Co-Ge QCs

(Al-Fe)B (x, y)	Al-Cu-Co-Ge (x, y)
397.730, -1 241.600	377.848, -1 171.396
1 053.900, -754.590	1 001.279, -724.595
-426.190, -1 244.700	-401.024, -1 162.569
639.120, -905.370	232.492, -722.191
-15.406, -1 112.900	621.903, -448.169
237.670, -760.820	-239.583, -730.166
648.460, -494.090	1 237.392, 0.042
1 057.300, -351.490	142.768, -428.748
-670.180, -904.740	-1 012.823, -721.914
-249.450, -763.180	370.742, -264.184
1 308.800, 1.332	774.302, 1.784
-1 068.700, -757.330	-633.800, -437.996
825.670, -2.435	449.169, 15.813
-666.080, -493.380	-155.888, -435.158
-1 076.600, -353.700	386.923, 279.638
-824.670, -2.078	-467.540, 4.226
663.940, 494.710	629.205, 459.153
1 071.800, 755.790	-777.861, 11.832
-1 308.900, -0.064	1 005.128, 737.354
249.010, 756.900	-1 237.416, -0.037
-1 068.300, 329.500	146.136, 434.121
657.790, 893.100	-373.041, 294.579
-651.840, 486.270	-147.625, 457.247
1 069.800, 343.660	240.477, 757.007
-237.780, 757.230	-622.395, 462.135
426.370, 1 229.800	-228.139, 744.928
-1057.300, 753.250	402.721, 1 188.463
14.080, 1 092.600	-996.987, 739.442
-650.560, 887.210	-362.601, 1 190.915
-391.750, 1 243.700	-389.080, -269.553

Table 2 Calculated Center Coordinates(pixels) of the (Perturbed) Diffraction Circles of the $Al_{80}Mn_{20}$ and Al-Mn QCs

$Al_{80}Mn_{20}$ (x, y)	Al-Mn (x, y)
395.050, -1 183.067	4.110, -1 223.854
-385.287, -1 182.986	667.341, -992.137
1 024.772, -734.136	305.282, -982.948
239.919, -733.153	-288.120, -994.248
-237.586, -732.784	-667.182, -989.807
-1 017.746, -735.397	804.618, -607.068
633.798, -451.208	199.139, -613.356
152.909, -448.846	-170.367, -603.336
-148.130, -449.523	-759.491, -616.661
-625.974, -451.987	1 092.062, -369.269
385.865, -286.879	496.819, -374.857
-387.871, -283.152	-474.447, -378.076
1 260.784, -0.048	-1 070.179, -394.019
779.861, -0.238	995.181, 5.202
473.820, 1.714	617.925, 6.883
-477.169, 1.680	-578.823, -10.194
-781.758, 1.589	-947.603, -6.761
-1 260.747, -0.004	1 122.523, 397.190
385.363, 279.579	512.380, 381.910
-389.602, 281.544	-455.740, 374.485
624.404, 447.180	817.055, 620.723
145.641, 443.306	-1 052.684, 361.694
-152.201, 444.358	214.867, 608.345
-631.979, 447.649	-152.143, 617.380
1 018.926, 733.141	-757.789, 604.395
236.660, 730.334	713.248, 994.736
-241.836, 730.737	345.493, 998.783
-1 023.111, 732.947	-255.557, 986.515
389.012, 1 180.931	-639.444, 997.138
-396.007, 1 181.220	36.094, 1 230.859